Journal of Power Sources 273 (2015) 959–965

Contents lists available at ScienceDirect

Journal of Power Sources

journal homepage: www.elsevier.com/locate/jpowsour

Enhanced cycle stability at high rate and excellent high rate capability of $La_{0.7}Sr_{0.3}Mn_{0.7}Co_{0.3}O_3$-coated $LiMn_2O_4$

Ting Shi, Yue Dong, Chun-Mei Wang, Fen Tao, Li Chen*

Department of Chemistry, School of Science, Tianjin University, Tianjin 300072, People's Republic of China

HIGHLIGHTS

- Electrochemical performance of $LiMn_2O_4$ is improved by $La_{0.7}Sr_{0.3}Mn_{0.7}Co_{0.3}O_3$ coating.
- 3 wt.% $La_{0.7}Sr_{0.3}Mn_{0.7}Co_{0.3}O_3$ coated $LiMn_2O_4$ shows excellent cycling stability.
- Outstanding high rate capability is obtained with $La_{0.7}Sr_{0.3}Mn_{0.7}Co_{0.3}O_3$ coating.
- The kinetics of electrodes is improved by $La_{0.7}Sr_{0.3}Mn_{0.7}Co_{0.3}O_3$ coating layer.

ARTICLE INFO

Article history:
Received 23 June 2014
Received in revised form
28 September 2014
Accepted 29 September 2014
Available online 7 October 2014

Keywords:
Spinel lithium manganese oxide
Strontium and cobalt co-doped lanthanum manganite
Excellent cycle stability
High rate capability

ABSTRACT

$La_{0.7}Sr_{0.3}Mn_{0.7}Co_{0.3}O_3$-coated spinel $LiMn_2O_4$ with excellent cycle stability and high rate capability is successfully prepared by a sol–gel method. The 3 wt.% $La_{0.7}Sr_{0.3}Mn_{0.7}Co_{0.3}O_3$-coated $LiMn_2O_4$ shows the optimum electrochemical performance. It can deliver 101 mAh g^{-1} at 10 C even after 100 cycles with a capacity retention of 93.5%. In contrast, the bare $LiMn_2O_4$ delivers 83.6 mAh g^{-1} at the same condition, only 84.5% capacity left. The rate capability of 3 wt.% $La_{0.7}Sr_{0.3}Mn_{0.7}Co_{0.3}O_3$-coated $LiMn_2O_4$ is also obviously enhanced, especially at high rates (10 C, 20 C and 30 C). It can deliver 74.3 mAh g^{-1} at 30 C which is much higher than that of the bare sample (47.2 mAh g^{-1}). The bare and coated $LiMn_2O_4$ samples are studied with various techniques. Both powder X-ray diffraction (XRD) and X-ray photoelectron spectroscopy (XPS) measurements demonstrate the existence of the $La_{0.7}Sr_{0.3}Mn_{0.7}Co_{0.3}O_3$, and it has no influence on the crystal structure of the pristine $LiMn_2O_4$. Transmission electron microscopy (TEM) shows that $La_{0.7}Sr_{0.3}Mn_{0.7}Co_{0.3}O_3$ coating layer with good crystallinity can cover the surface of $LiMn_2O_4$ to form a core–shell structure. Electrochemical impedance spectroscopy (EIS) and cyclic voltammetry (CV) demonstrate that the coating layer can improve the kinetics of electrodes.

1. Introduction

Spinel $LiMn_2O_4$ is a promising cathode material due to excellent voltage profile characteristics, high safety, low cost, acceptable environmental impact, non-toxicity and easy fabrication [1–4]. However, its cycle stability and rate capability are still poor for practical application. The poor cycle stability is mainly ascribed to the slow dissolution of manganese, electrolyte decomposition and Jahn–Teller distortion [5,6]. The poor rate capability is related to low electronic and ionic conductivity of pristine $LiMn_2O_4$, as well as slow diffusion of lithium ions at the cathode/electrolyte interface [7,8].

Surface modification has been proved to be an effective approach to overcome these obstacles. The coating layer acts as not only a physical protection barrier to isolate the cathode materials from the electrolyte, but also an HF scavenger to decrease the acidity of electrolyte and impede the manganese dissolution from $LiMn_2O_4$ [9]. Therefore, the coating layer can help to achieve good cyclability during the charge–discharge process, as well as suppress the side reactions between cathode materials and electrolyte. Furthermore, an electronic conductive coating layer (electron-conducting media) that facilitates the charge transfer can also greatly improve the discharge capacity and rate capability at high discharge rates. For example, Huang et al. [10] found that a silver coating layer greatly enhanced the electronic conductivity and discharge capacity of $LiMn_2O_4$ at 8 C and 10 C. In addition, the perovskite-type oxide with high electronic conductivity is also a good candidate of coating materials. Cui et al. [11] reported that

* Corresponding author. Tel.: +86 22 27892379; fax: +86 22 27403475.
E-mail address: chenli_su@eyou.com (L. Chen).

http://dx.doi.org/10.1016/j.jpowsour.2014.09.183
0378-7753/

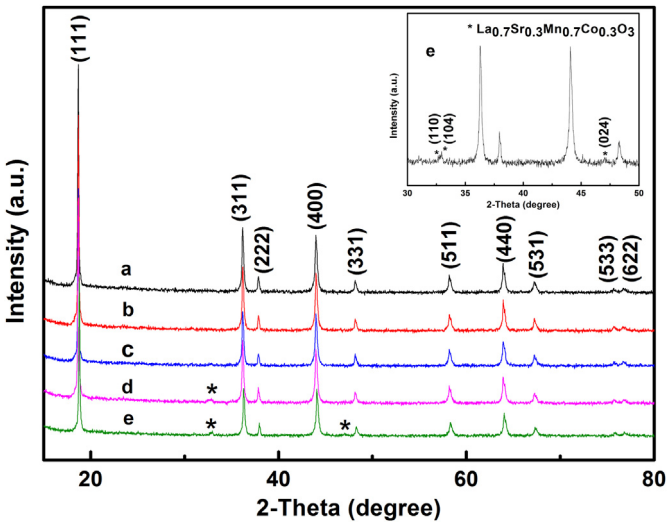

Fig. 1. X-ray diffraction patterns of (a) sample-0, (b) sample-1, (c) sample-2, (d) sample-3 and (e) sample-4, inset: partially magnified XRD patterns of e.

$La_{0.7}Sr_{0.3}MnO_3$ and carbon co-coated $LiFePO_4$ showed high discharge capacities at 0.5 C and 1 C. Zhao et al. [12] also proposed that a $La_{0.7}Sr_{0.3}MnO_3$ coating layer effectively enhanced the thermal storage and rate capability of $LiNi_{0.5}Mn_{1.5}O_4$.

In this study, the perovskite-type oxide $La_{0.7}Sr_{0.3}Mn_{0.7}Co_{0.3}O_3$ is coated on the surface of $LiMn_2O_4$ powders, and the electrochemical performances of $La_{0.7}Sr_{0.3}Mn_{0.7}Co_{0.3}O_3$-coated $LiMn_2O_4$ materials are systematically investigated.

2. Experimental

$La_{0.7}Sr_{0.3}Mn_{0.7}Co_{0.3}O_3$-coated $LiMn_2O_4$ samples were prepared by a sol–gel process. All raw materials were analytical-grade. $La(NO_3)_3\cdot 6H_2O$, $Sr(NO_3)_2\cdot 2H_2O$, $Mn(NO_3)_2\cdot 6H_2O$ and $Co(NO_3)_2\cdot 6H_2O$ in stoichiometric amounts were dissolved in distilled water, and the total molar concentration of all metal ions is 0.2 mol L^{-1}. $C_6H_8O_7\cdot H_2O$ was added into the solution as complexation agent, and its molar concentration is 0.3 mol L^{-1}. $NH_3\cdot H_2O$ was used to adjust the pH value of the above solution to 3. The obtained solution was heated at 60 °C to form a homogeneous sol under continuous stirring. Then the commercial $LiMn_2O_4$ powders (Tianjin Huaxia Hongyuan industrial Co., ltd.) were added into the sol and stirred vigorously for 10 h. The amounts of $La_{0.7}Sr_{0.3}Mn_{0.7}Co_{0.3}O_3$ in the sol were set to 1, 2, 3 and 4 wt.% of the $LiMn_2O_4$ powders, respectively. After drying at 120 °C for 10 h, the resulting mixture was calcined at 400 °C for 4 h and 700 °C for 10 h in sequence to obtain the coated $LiMn_2O_4$ cathode materials. The samples with about 1, 2, 3 and 4 wt.% $La_{0.7}Sr_{0.3}Mn_{0.7}Co_{0.3}O_3$ were respectively designated as sample-1, 2, 3, 4, and the bare $LiMn_2O_4$ was designated as sample-0.

The structure properties of all samples were investigated by Powder X-ray diffraction (XRD, D/max 2500 V/PC, Rigaku, 40 KV, 150 mA) using Cu-Kα radiation ($\lambda = 1.5405$ Å) and a bent graphite monochromatic from 10° to 80° at a scan speed of 2° min^{-1}. The morphologies and microstructures of the samples were examined by transmission electron microscopy (TEM, JEM-2100F, JEOL 200 KV). The surface chemical compositions of the samples were measured by X-ray photoelectron spectroscopy (XPS, AXIS Ultra DLD, Kratos) using Al Kα radiation (1486.6 eV). The binding energies were calibrated by referencing the C1s line at 284.6 eV.

Electrode slurry was prepared by mixing active materials, carbon black and polyvinylidene fluoride (PVDF) at a weight ratio of 8:1:1 in *N*-methyl-2 pyrrolidine (NMP) solvent, then it was coated on aluminum foil and dried at 120 °C for 12 h under vacuum. The dried electrode was further punched into round disk with a diameter of 1.2 cm and subsequently rolled into a thin film with a thickness of 32 μm. The amount of active material in each disk is the same. The coin cells (CR2032) were assembled in an argon-filled glove box using the obtained electrode as the cathode, lithium foil as the counter electrode and 1 M $LiPF_6$ in EC/DEC/EMC (1:1:1 by volume) as the electrolyte. Then the cells were measured by a battery testing system (CT2001A, LAND) between 3.0 and 4.3 V at different rates (1 C = 120 mA g^{-1}). The electrochemical impedance spectroscopy (EIS) analysis was performed on an electrochemical workstation PARSTAT 2273 in the frequency range from 10 mHz to 100 kHz and an ±5 mV AC signal. Cyclic voltammetry (CV) tests were carried out between 3.0 and 4.3 V vs. Li/Li^+ at a scan rate of 0.1 mV s^{-1} using an electrochemical workstation (CHI 600E).

3. Results and discussion

Fig. 1 shows the XRD patterns of the bare and $La_{0.7}Sr_{0.3}Mn_{0.7}Co_{0.3}O_3$ coated samples. The sharp diffraction peaks in Fig. 1 demonstrate that all the samples have good crystal structure. The XRD patterns of all samples can be well indexed to the standard cubic spinel structure with $Fd\bar{3}m$ space group (JCPDS Card No. 35-0782). In this structure, the oxygen ions in 32e sites form a cubic closed-packed lattice, while lithium ions and manganese ions respectively occupy the tetrahedral (8a) sites and the octahedral (16d) sites. The adjacent vacant octahedral (16c) sites form a three-dimensional lithium ions diffusion pathway. However, the XRD

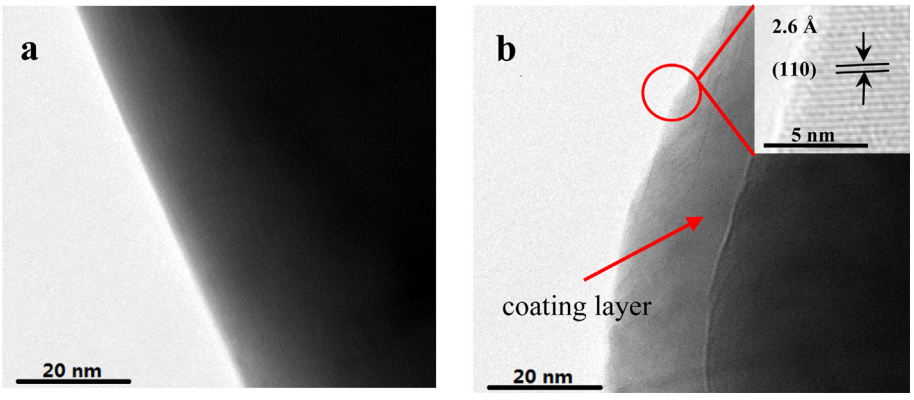

Fig. 2. TEM images of (a) sample-0 and (b) sample-3 before cycling.

patterns for sample-3 and sample-4 also present some weak peaks of a second phase (marked as *). The amplified pattern in the 2θ range of 30–50° for sample-4 in the inset of Fig. 1 shows the diffraction peaks of (110), (104) and (024) for $La_{0.7}Sr_{0.3}Mn_{0.7}Co_{0.3}O_3$, which is assigned to a rhombohedral structure with $R\bar{3}c$ space group [13]. So the peaks indicate the existence of $La_{0.7}Sr_{0.3}Mn_{0.7}Co_{0.3}O_3$ particles in the composite. With increasing the amount of $La_{0.7}Sr_{0.3}Mn_{0.7}Co_{0.3}O_3$, the diffraction peaks corresponding to $La_{0.7}Sr_{0.3}Mn_{0.7}Co_{0.3}O_3$ become stronger, but the diffraction peaks of $LiMn_2O_4$ have no change. Therefore, $La_{0.7}Sr_{0.3}Mn_{0.7}Co_{0.3}O_3$ modification has no influence on the spinel structure of $LiMn_2O_4$.

The TEM images of sample-0 and sample-3 particle before cycling are shown in Fig. 2. Compared with the smooth surface of sample-0 particle in Fig. 2a, a coating layer can be distinctly observed on the surface of sample-3 particle in Fig. 2b. Furthermore, the inset of Fig. 2b clearly shows the lattice fringe patterns with a lattice spacing of 2.6 Å assigned to the (110) planes of $La_{0.7}Sr_{0.3}Mn_{0.7}Co_{0.3}O_3$ crystallites, which confirms that the

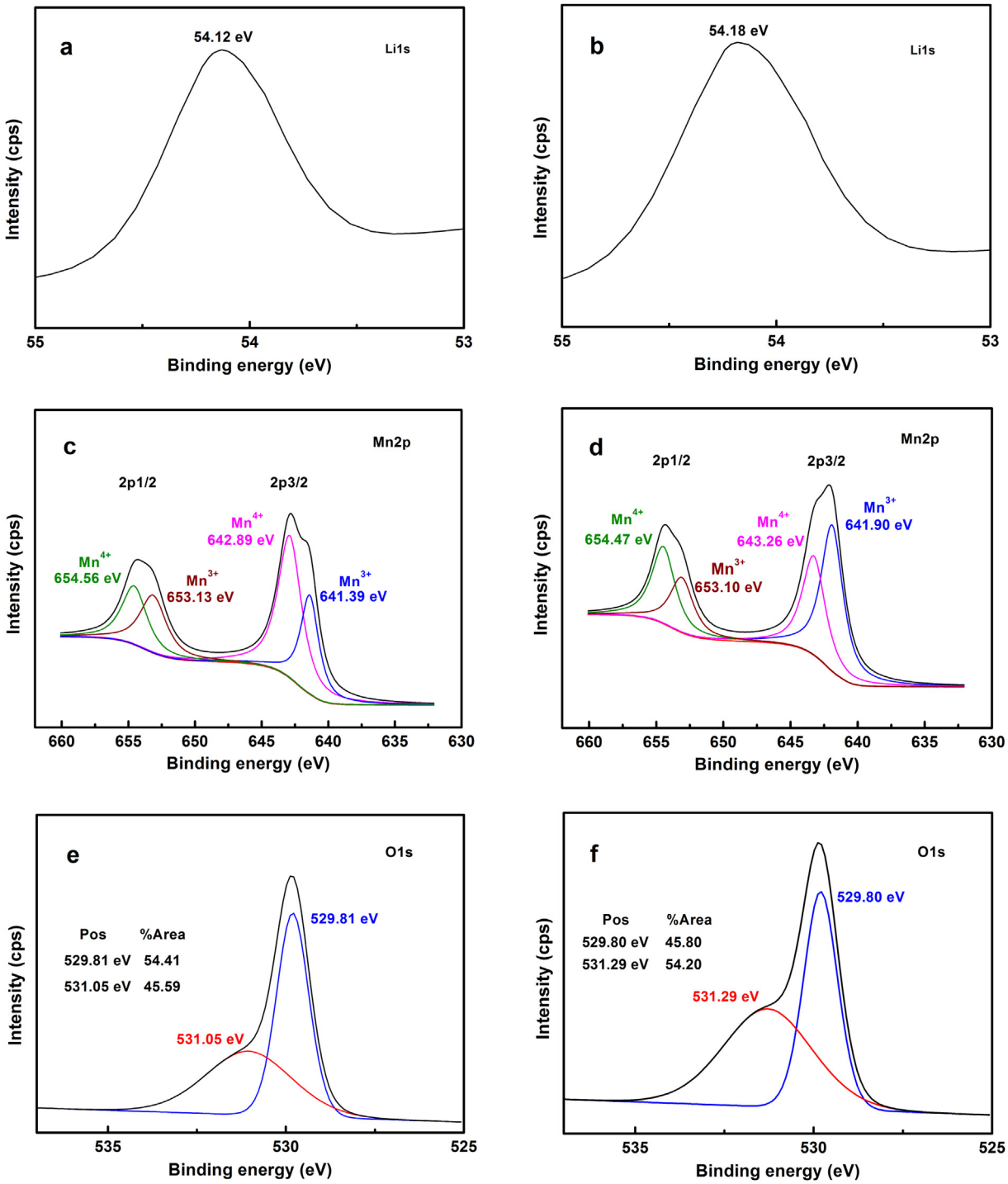

Fig. 3. XPS spectra of (a, c, e) sample-0 and (b, d, f) sample-3. (a, b) Li1s spectra; (c, d) Mn2p spectra; (e, f) O1s spectra.

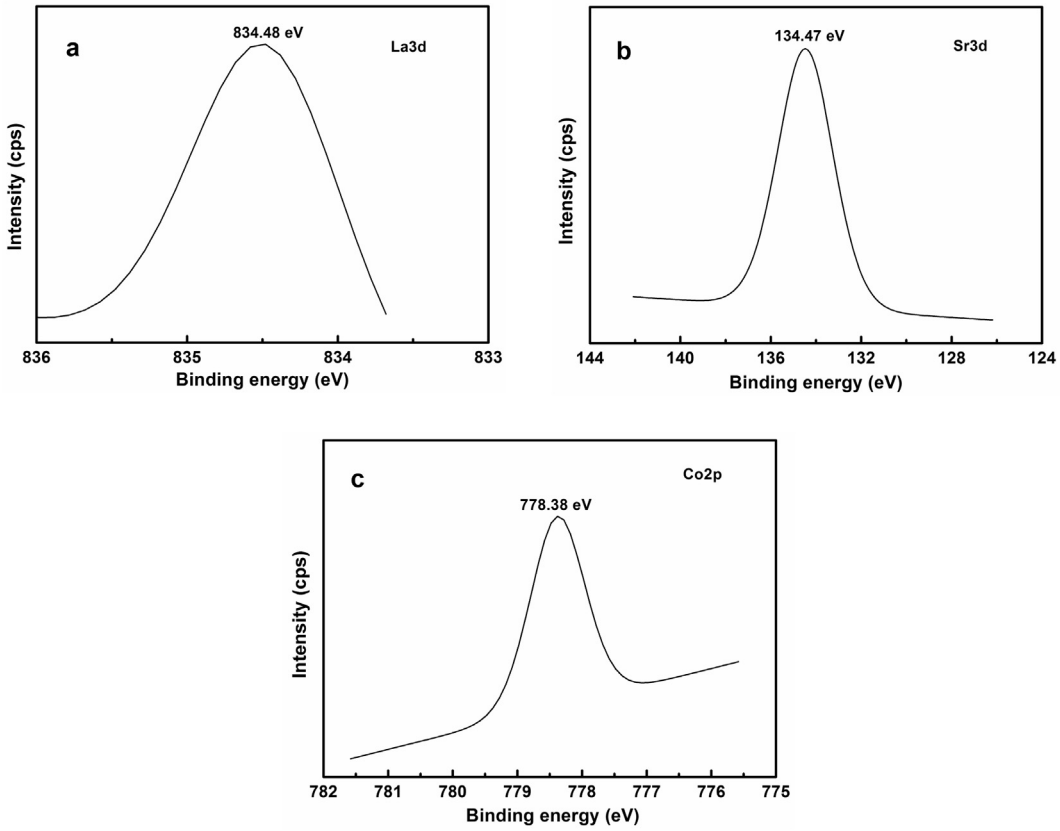

Fig. 4. XPS spectra of sample-3. (a) La3d spectrum; (b) Sr3d spectrum; (c) Co2p spectrum.

$La_{0.7}Sr_{0.3}Mn_{0.7}Co_{0.3}O_3$ with high crystallinity covers the surface of $LiMn_2O_4$. From the TEM images, we could infer that a core–shell structure is formed, which benefits to improve the electrochemical performance of the core material [9,14].

The XPS spectra of Li1s, Mn2p and O1s for sample-0 and sample-3 are given in Fig. 3. The Li1s peaks at binding energies of 54.12 eV (Fig. 3a) and 54.18 eV (Fig. 3b) are in good agreement with the signal of lithium in the $LiMn_2O_4$ crystalline network [15]. The existence of Li1s peak in sample-3 is caused by the inhomogeneous coating layer of $La_{0.7}Sr_{0.3}Mn_{0.7}Co_{0.3}O_3$, whose thickness varies within a certain range. So it is possible that the Li1s peak can be detected in the thinner zones which are in the detection range of XPS measurements. The XPS spectra of Mn2p can be decomposed into two components ($Mn2p_{3/2}$ and $Mn2p_{1/2}$) due to the spin–orbital splitting [16]. For sample-0 (Fig. 3c), the observed values of the binding energies for Mn^{3+} are 641.39 eV ($Mn2p_{3/2}$) and 653.13 eV ($Mn2p_{1/2}$), while those of Mn^{4+} are 642.89 eV ($Mn2p_{3/2}$) and 654.56 eV ($Mn2p_{1/2}$). For sample-3 (Fig. 3d), both the peak at 641.90 eV ($Mn2p_{3/2}$) and the peak at 653.10 eV ($Mn2p_{1/2}$)

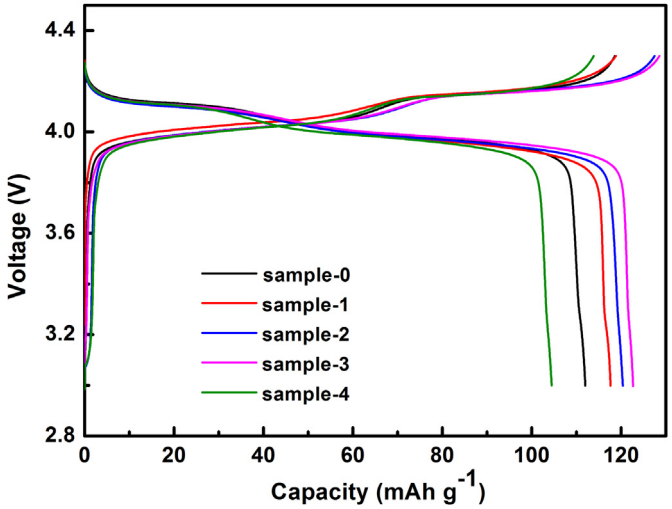

Fig. 5. Initial charge–discharge curves of all samples at 0.2 C between 3.0 and 4.3 V.

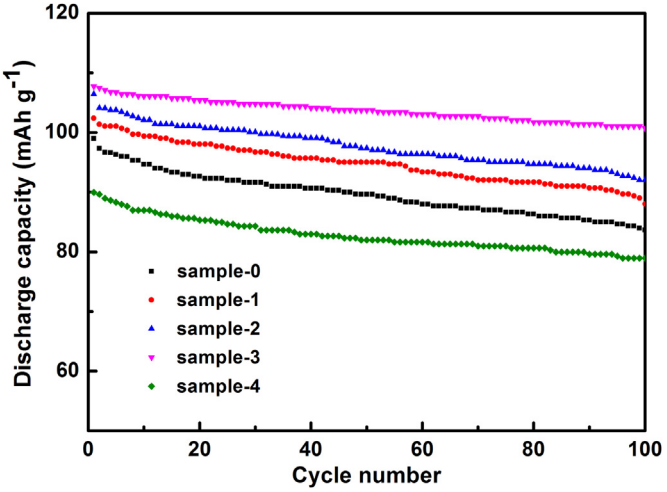

Fig. 6. Cycle performance of all samples at 10 C between 3.0 and 4.3 V.

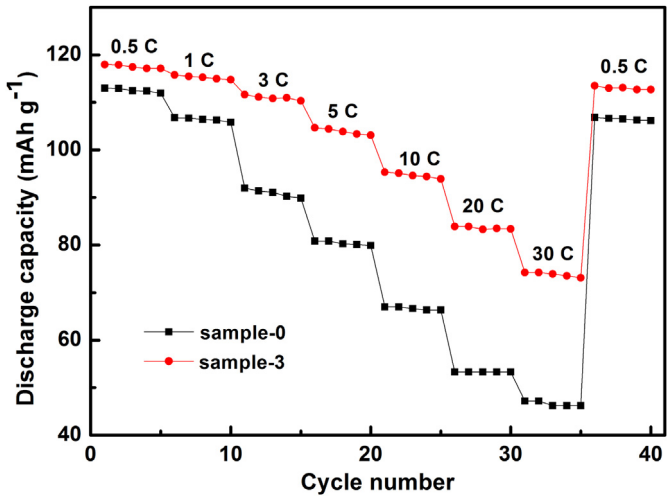

Fig. 7. Rate capability of sample-0 and sample-3 from 0.5 C to 30 C between 3.0 and 4.3 V.

are assigned to Mn^{3+}, and the other peaks at 643.26 eV ($Mn2p_{3/2}$) and 654.47 eV ($Mn2p_{1/2}$) correspond to the Mn^{4+} [17]. After coating, the peaks of $Mn2p_{3/2}$ for sample-3 both shift toward the higher binding energies, which is caused by the manganese in the $La_{0.7}Sr_{0.3}Mn_{0.7}Co_{0.3}O_3$ coating layer. The O1s spectra (Fig. 3e and f) indicate there exist two different kinds of oxygen species in the samples. The peaks at 529.81 eV (Fig. 3e) and 529.80 eV (Fig. 3f) can be attributed to lattice oxygen, while the other peaks at 531.05 eV (Fig. 3e) and 531.29 eV (Fig. 3f) are ascribed to oxygen adsorbed at the surface [18,19]. The calculated atom ratio of adsorbed oxygen to lattice oxygen in sample-3 is higher than that in sample-0. Moreover, the change of binding energy for adsorbed oxygen (0.24 eV) is larger than that of lattice oxygen (0.01 eV) after coating. So the coating layer has a large influence on the oxygen chemisorption state on the surface of sample-3 [20].

For sample-3, the XPS spectra of La3d, Sr3d and Co2p can also be observed. The characteristic binding energy at 834.48 eV in Fig. 4a can be assigned to $La3d_{5/2}$ [21]. The peak around 134.47 eV in Fig. 4b corresponds to $Sr3d_{5/2}$ [22]. The main peak at 778.38 eV in Fig. 4c agrees with that of $Co2p_{3/2}$ [23]. So the existences of La, Sr and Co elements on sample-3 surface can be confirmed by the above spectra. From the differences of the XPS spectra, we can infer that a new substance is formed on the $LiMn_2O_4$ surface, which has been confirmed to be $La_{0.7}Sr_{0.3}Mn_{0.7}Co_{0.3}O_3$ by XRD results.

Fig. 5 presents the initial charge–discharge curves of all samples at 0.2 C. The initial discharge capacity of sample-0 is 112 mAh g^{-1}, while those of sample-1, sample-2, sample-3 and sample-4 are 118, 120, 123, and 104 mAh g^{-1} in sequence. Obviously, the discharge capacities of coated samples, except sample-4, are higher than that of sample-0. So a moderate surface coating amount can help to deliver a higher discharge capacity due to the high electronic conductivity of $La_{0.7}Sr_{0.3}Mn_{0.7}Co_{0.3}O_3$. As $La_{0.7}Sr_{0.3}Mn_{0.7}Co_{0.3}O_3$ is inactive, the excess coating amount can lower the lithium ions diffusion at the interface of electrode/electrolyte [24]. Thus, sample-4 shows a poor electrochemical performance.

According to the corresponding reports [25], both the insertion and the extraction of lithium ions proceed in terms of the following two reversible reactions:

$$\frac{1}{2}Li^+ + \frac{1}{2}e + 2\lambda - MnO_2 \underset{\text{charge}}{\overset{\text{discharge}}{\rightleftharpoons}} Li_{0.5}Mn_2O_4$$

$$\frac{1}{2}Li^+ + \frac{1}{2}e + Li_{0.5}Mn_2O_4 \underset{\text{charge}}{\overset{\text{discharge}}{\rightleftharpoons}} LiMn_2O_4$$

The reversible Mn^{3+}/Mn^{4+} redox reactions above occur concurrently. All our samples distinctly show two characteristic voltage plateaus of well defined spinel $LiMn_2O_4$ approximately at 4.1 and 4.0 V, which suggests $La_{0.7}Sr_{0.3}Mn_{0.7}Co_{0.3}O_3$ coating layer has no influence on the intrinsic properties of $LiMn_2O_4$. Hence, the surface coating can't change the crystal structure of $LiMn_2O_4$, but it can help to improve charge–discharge properties. The results can be further supported by the following tests.

The cycle performances of all samples are further compared in Fig. 6. The cells are charged at 1 C and discharged at 10 C for 100 cycles. The discharge capacity of sample-0 decreases from 99.0 to 83.6 mAh g^{-1} after 100 cycles with a capacity retention of 84.5%. In contrast, the coated samples respectively exhibit initial discharge capacities of 102, 106, 108 and 90.0 mAh g^{-1} at 10 C, and the corresponding capacity retentions are 86.0%, 86.5%, 93.5% and 87.8% in sequence after 100 cycles. Obviously, all the coated samples display more excellent cycle performance than the bare one, and sample-3 shows the highest discharge capacity and capacity retention among the five samples.

According to the previous reports [5,26], the capacity fading of $LiMn_2O_4$ is mainly caused by manganese dissolution into the electrolyte from the active materials during extensive cycling due to the existence of HF in the electrolyte. So we think that $La_{0.7}Sr_{0.3}Mn_{0.7}Co_{0.3}O_3$ coating layer can effectively suppress the manganese dissolution [12,27] by preventing the direct contact

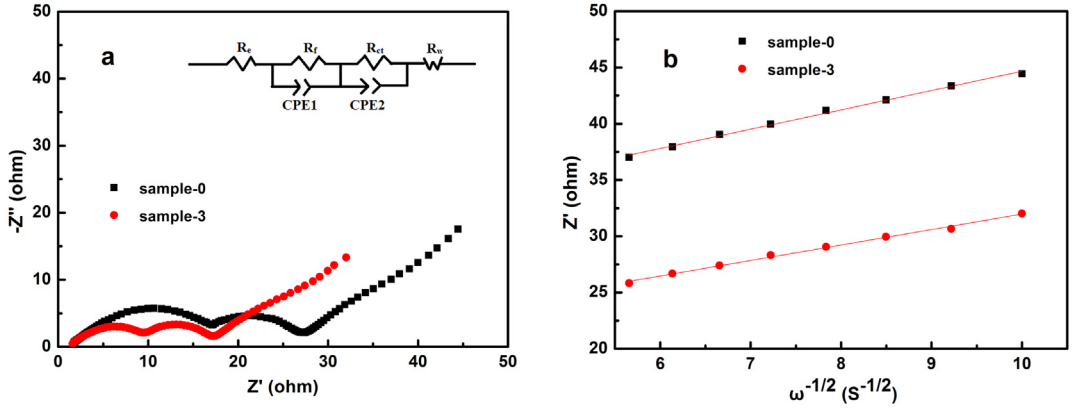

Fig. 8. (a) The EIS plots of sample-0 and sample-3, inset: the equivalent circuit for EIS results fitting, and (b) the relationship between Z' and $\omega^{-1/2}$ in low frequency.

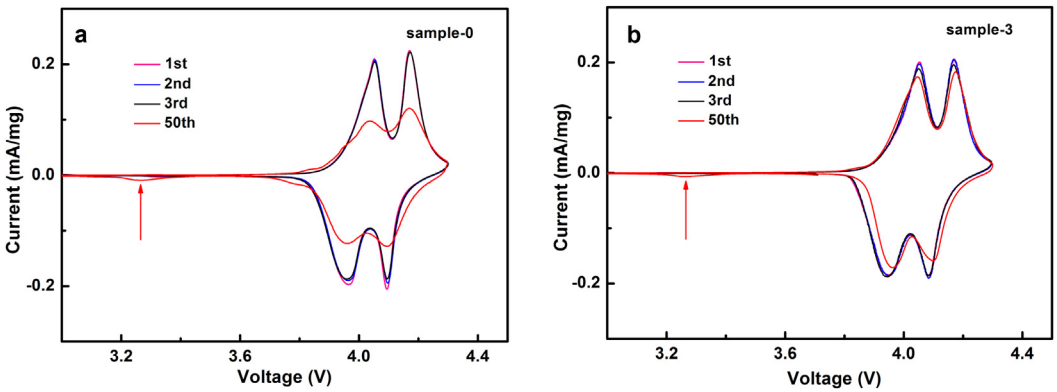

Fig. 9. CV curves between 3.0 and 4.3 V with a scan rate of 0.1 mV s^{-1} of (a) sample-0 and (b) sample-3.

between bulk $LiMn_2O_4$ and HF in electrolyte. Correspondingly, the cycle performance is improved.

Fig. 7 shows the rate capabilities of sample-0 and sample-3. The cells are first cycled at 0.5 C, then charged at 1 C and discharged at 1 C, 3 C, 5 C, 10 C and 30 C, respectively, and finally cycled at 0.5 C again (five times at each rate). Sample-3 visibly exhibits much better rate capability than sample-0 at any rates, especially at high rates (10 C, 20 C and 30 C). The discharge capacities of sample-0 and sample-3 at 0.5 C are similar, which are 113 mAh g^{-1} and 118 mAh g^{-1}, respectively, but the discharge capacity of sample-0 decreases much more rapidly than that of sample-3 with increasing the discharge rate. Sample-3 can deliver 74.3 mAh g^{-1} at 30 C which is 63.0% of the initial capacity at 0.5 C, but the discharge capacity of sample-0 at 30 C is only 47.2 mAh g^{-1} which is 41.8% of the initial capacity at 0.5 C. The capacity recovery after 30 C for sample-3 is nearly 97.4%, which is also higher than that of sample-0 (96.1%).

The better rate capability can still be accounted for the high electronic conductivity of $La_{0.7}Sr_{0.3}Mn_{0.7}Co_{0.3}O_3$ (about 100 S cm^{-1}) [7,8,12]. Because the coating layer can not only reduce the inter-particle resistance and facilitate heterogeneous charge transfer process on the cathode surface, but also provide the extra electron-conducting pathways among the particles as well as between the current collector and the material particles [9].

Fig. 8 displays the Nyquist plots of sample-0 and sample-3 after 50 cycles (charged at 1 C and discharged at 10 C). The equivalent circuit is also shown in the inset of Fig. 8a. All the spectra in Fig. 8a are composed of two depressed semicircles in the high-to-medium frequency and an inclined line in the low frequency. The high frequency intercept at the real axis corresponds to the ohmic resistance (R_e) of the cell, mainly contributed from the electrolyte. The high-frequency depressed semicircle is attributed to the resistance of lithium ions migration through surface layers (R_f) [28]. The medium-frequency depressed semicircle originates from the charge transfer resistance (R_{ct}) between inter-particles [29]. The inclined line is related to the Warburg impedance (R_w) [30].

The diffusion coefficient D_{Li^+} is calculated according to the following equation [20,31]:

$$D_{Li^+} = \frac{R^2T^2}{2A^2n^4F^4c^2\sigma^2}$$

where R is the gas constant (8.314 J mol^{-1} K^{-1}), T is the temperature (298.15 K), A is the surface area of the electrode, n is the number of shifted electrons, F is the Faraday constant (96,500 C mol^{-1}), c is the molar concentration of lithium ions, and σ is the Warburg coefficient which can be obtained from the plot slope of Z' vs. $\omega^{-1/2}$ (the reciprocal root square of the lower angular frequencies) [11,31]. The corresponding plots of Z' vs. $\omega^{-1/2}$ are shown in Fig. 8b.

The equivalent circuit parameters R_e, R_f and R_{ct} are also calculated, which are 1.462 Ω, 19.01 Ω and 4.499 Ω for sample-0 and 1.382 Ω, 9.885 Ω and 4.046 Ω for sample-3, respectively. The calculated resistances of sample-3 are all smaller in comparison with those of sample-0, which indicates the coating layer can reduce the electrodes' resistances and improve their kinetics, resulting in the excellent high rate capability of sample-3 [7,28]. The D_{Li^+} value of sample-3 is 2.15×10^{-10} cm^2 s^{-1} which is higher than that of sample-0 (1.38×10^{-10} cm^2 s^{-1}). The result above indicates that $La_{0.7}Sr_{0.3}Mn_{0.7}Co_{0.3}O_3$ coating layer can facilitate

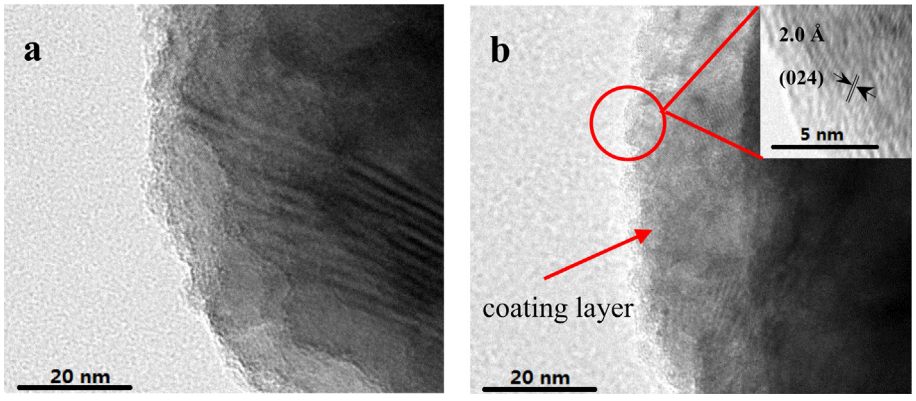

Fig. 10. TEM images of (a) sample-0 and (b) sample-3 after 50 cycles.

lithium ions diffusion at the interface, which is also beneficial to improve the rate capability.

The CV curves of sample-0 and sample-3 after activated at 0.1 C are presented in Fig. 9. The first three consecutive CVs of both samples show the similar couples of well-defined redox peaks of the spinel $LiMn_2O_4$ [13]. After 50 cycles at 10 C, the CV peaks related to sample-0 become much broader compared to the peaks of sample-3, which suggests the kinetics of sample-0 is much slower than that of sample-3 [28]. The CV results correlate well with the EIS results. In addition, the relative intensities of major redox peaks for sample-0 decrease much more sharply than those of sample-3, which means that the $La_{0.7}Sr_{0.3}Mn_{0.7}Co_{0.3}O_3$ coating layer is beneficial to maintain the stable electrochemical performance of $LiMn_2O_4$. Additionally, the small reduction peaks appeared at about 3.3 V in the CVs are related to the formation of double hexagonal-type layers, which corresponds to the reversible migration of manganese ions from 16d to 16c sites. Hence, $La_{0.7}Sr_{0.3}Mn_{0.7}Co_{0.3}O_3$ coating layer cannot suppress the spinel-to-double hexagonal phase transition [5].

TEM images of sample-0 and sample-3 after 50 cycles (charged at 1 C and discharge at 10 C) are given in Fig. 10. For cycled sample-3 particle (Fig. 10b), the $La_{0.7}Sr_{0.3}Mn_{0.7}Co_{0.3}O_3$ coating layer with lattice fringes of (024) planes can still be visibly observed on $LiMn_2O_4$ surface, which indicates that the $La_{0.7}Sr_{0.3}Mn_{0.7}Co_{0.3}O_3$ coating layer can effectively protect the bulk $LiMn_2O_4$ from electrolyte attack. However, the smooth surface of sample-0 particle (Fig. 2a) has become microscopically rough (Fig. 10a) after cycling, which suggests that sample-0 surface has been damaged during charge/discharge processes [32]. So we infer that $La_{0.7}Sr_{0.3}Mn_{0.7}Co_{0.3}O_3$ can successfully act as a physical protection layer to restrain the reactions between $LiMn_2O_4$ and electrolyte [9,20]. Consequently, the existence of $La_{0.7}Sr_{0.3}Mn_{0.7}Co_{0.3}O_3$ coating layer can help to enhance the structure stability of $LiMn_2O_4$ during cycling, which finally leads to the excellent cycle stability of sample-3.

4. Conclusions

$La_{0.7}Sr_{0.3}Mn_{0.7}Co_{0.3}O_3$-coated $LiMn_2O_4$ materials with a core–shell structure exhibit enhanced cycle stability at high discharge rate and excellent high rate capability. The 3 wt.% $La_{0.7}Sr_{0.3}Mn_{0.7}Co_{0.3}O_3$-coated $LiMn_2O_4$ gives the highest discharge capacity and excellent rate capability, whose capacity retention retains 93.5% even after 100 cycles at 10 C between 3.0 and 4.3 V. The improved electrochemical performance can be attributed to the stable $La_{0.7}Sr_{0.3}Mn_{0.7}Co_{0.3}O_3$ coating layer which can enhance the electronic conductivity, prevent the direct contact between bulk $LiMn_2O_4$ and HF in electrolyte and improve the kinetics of electrodes. Therefore, the $La_{0.7}Sr_{0.3}Mn_{0.7}Co_{0.3}O_3$ coating is an effective way to overcome the existed obstacles of $LiMn_2O_4$ (poor cycle stability and rate capability) for the practical application.

Acknowledgment

The authors acknowledge the financial support of Tianjin Huaxia Hongyuan Industrial Co., Ltd.

References

[1] D. Kovacheva, H. Gadjov, K. Petrov, S. Mandal, M.G. Lazarraga, et al., J. Mater. Chem. 12 (2002) 1184–1188.
[2] X.X. Li, F.Y. Cheng, B. Guo, J. Chen, J. Phys. Chem. 109 (2005) 14017–14024.
[3] Y.K. Sun, C.S. Yoon, C.K. Kim, S.G. Youn, Y.S. Lee, et al., J. Mater. Chem. 11 (2001) 2519.
[4] F.Y. Cheng, H.B. Wang, Z.Q. Zhu, Y. Wang, et al., Energy Environ. Sci. 4 (2011) 3668–3675.
[5] Y.C. Sun, Z.X. Wang, L.Q. Chen, X.J. Huang, J. Electrochem. Soc. 150 (2003) A1294–A1298.
[6] M. Wohlfahrt-Mehrens, C. Vogler, J. Garche, J. Power Sources 127 (2004) 58–64.
[7] S.C. Park, Y.M. Kim, Y.M. Kang, K.T. Kim, P.S. Lee, J.Y. Lee, J. Power Sources 103 (2001) 86–92.
[8] H.L. Chen, C.P. Grey, Adv. Mater. 20 (2008) 2206–2210.
[9] Z.H. Chen, Y. Qin, K. Amine, Y.K. Sun, J. Mater. Chem. 20 (2010) 7606–7612.
[10] S.H. Huang, Z.Y. Wen, X.L. Yang, X.J. Zhu, B. Lin, Electrochem. Solid-State Lett. 9 (2006) A443–A447.
[11] Y. Cui, X.L. Zhao, R.S. Guo, Electrochim. Acta 55 (2010) 922–926.
[12] G.Y. Zhao, Y.B. Lin, T. Zhou, Y. Lin, Y.D. Huang, Z.G. Huang, J. Power Sources 215 (2012) 63–68.
[13] B.C. Zhao, W.H. Song, Y.Q. Ma, et al., Phys. Status Solidi B 242 (2005) 1719–1727.
[14] L.W. Su, Y. Jing, Z. Zhou, Nanoscale 3 (2011) 3967–3983.
[15] H.G. Zhang, Y.T. Li, X.G. Dong, Q.T. Hou, Y.C. Huang, H. Liu, Q. Li, J. Phys. 430 (2013) 012072.
[16] X.F. Chu, K.K. Huang, M. Han, S. Feng, Inorg. Chem. 52 (2013) 4130–4132.
[17] T. Hishida, K. Ohbayashi, M. Kobata, E. Ikenaga, T. Sugiyama, K. Kobayashi, M. Okawa, T. Saitoh, J. Appl. Phys. 113 (2013) 233702.
[18] H.X. Dai, C.F. Ng, C.T. Au, J. Catal. 189 (2000) 52–62.
[19] Q. Hu, C.C. Wu, L.Q. Cao, B. Chi, et al., J. Power Sources 226 (2013) 8–15.
[20] Y. Huang, F.M. Jin, F.J. Chen, L. Chen, J. Power Sources 256 (2014) 1–7.
[21] D. Arumugam, G. Paruthimal Kalaignan, Mater. Res. Bull. 45 (2010) 1825–1831.
[22] W.Q. Wang, J. Yang, Y.P. Gong, H.L. Hong, Mater. Res. Bull. 48 (2013) 21–24.
[23] P.H. Shi, R.J. Su, F.Z. Wan, M.C. Zhu, D.X. Li, S.H. Xu, Appl. Catal. 123–124 (2012) 265–272.
[24] X.Z. Liu, H.Q. Li, E. Yoo, M. Ishida, H.S. Zhou, Electrochim. Acta 83 (2012) 253–258.
[25] X.M. Wu, S. Chen, M.,Y. Ma, J.B. Liu, Ionics 17 (2011) 35–39.
[26] Y. Shaohorn, S.A. Hackney, A.J. Kahaian, K.D. Kepler, E. Skinner, J.T. Vaughey, M.M. Thackeray, J. Power Sources 81–82 (1999) 496–499.
[27] M.M. Thackeray, C.S. Johnson, J.S. Kim, K.C. Lauzze, J.T. Vaughey, et al., Electrochem. Commun. 5 (2003) 752–758.
[28] J.S. Gnanaraj, V.G. Pol, A. Gedanken, D. Aurbach, Electrochem. Commun. 5 (2003) 940–945.
[29] J. Fan, P.S. Fedkiw, J. Power Sources 72 (1998) 165–173.
[30] Y.L. Ma, Y.Z. Gao, P.J. Zuo, X.Q. Cheng, G.P. Yin, Int. J. Electrochem. Sci. 7 (2012) 11001–11010.
[31] Z.Q. Huo, Y.T. Cui, D. Wang, Y. Dong, L. Chen, J. Power Sources 245 (2014) 331–336.
[32] Y.K. Sun, C.S. Yoo, C.K. Kim, S.G. Youn, Y.S. Lee, M. Yoshio, I.H. Oh, J. Mater. Chem. 11 (2001) 2519–2522.